Indian Journal of Pure & Applied Physics
Vol. 61, July 2023, pp. 546-553
DOI: 10.56042/ijpap.v61i7.111

Efficient Coupling of Single Photons into Tilted Nanofiber Bragg Gratings

Subrat Sahu & Rajan Jha*

Nanophotonics and Plasmonics Laboratory, School of Basic Sciences, IIT Bhubaneswar, Khurda 752 050, Odisha, India

Received 17 October 2022; accepted 12 June 2023

We report a new gateway towards the light-matter interaction of spontaneous emission from a quantum emitter (QE) in optical nanofiber (ONF) based on nanocavities tilted by some angle with respect to the plane of the fiber cross-section. This structure is designed by three-dimensional finite-difference time-domain simulations to enhance the spontaneous emission decay rate from a QE and maximize the coupling efficiency into the fiber-guided modes. Here, we systematically analyzed the polarization-dependent spontaneous emission characteristics of QE and cavity characteristics of the proposed structure. We show that the coupling efficiency from single emitters can reach as high as ~ 90% with the Purcell factor can be as high as ~ 65. The results show a 10-fold enhancement factor from a QE in the cavity center compared with the cavity surface. The tilted angle can be optimized to get more transmission and coupling efficiency. This tilted structure has a high *Q*-factor of ~ 1000 and a low mode volume of ~ 0.56 μm^3, with a maximum degree of polarization of the single photons has been calculated as high as 96%. For the quantum information and quantum photonics application, this system attracts researchers to a new direction in the quantum world.

Keywords: Tilted fiber Bragg grating; Single Photon; cQED

1 Introduction

Efficient and robust light-matter interaction plays an essential role in the quantum systems to control the coupling of photons emitted from the quantum emitters (QEs) for a variety of applications[1–4]. Optical nanofiber (ONF), a sub-wavelength diameter of single mode fiber (SMF) emerges as an efficient and configurable interface/workbench for such QEs to study light-matter interaction[4–6] due to its tight confinement of the high-intensity transverse mode around the fiber. The photons emitted from the QEs placed over the ONF can be precisely coupled to the guided modes via a strong evanescent field and to the free space through radiation mode. In the recent past, the coupling of light emitters with the ONF had experimentally been investigated using neutral atoms[7], semiconductor quantum dots at room temperature[8] also at a cryogenic temperature[9], molecules[10], nitrogen-vacancy (NV) in diamond[11–13], and 2D materials[14]. The maximum coupling efficiency of 30% has been calculated by placing an NV center on the surface of ONF[12]. However, it has been analytically estimated that 28% of the quantum lights can be channeled into the guided modes of ONF from Cesium atoms[15]. Experimentally, 22 % of photons from the single QE have been coupled to the guided mode of ONF by precisely positioning the QEs on the surface of ONF[8].

To further increase the spontaneous emission rate and coupling efficiency, systems like micropillar cavities using distributed Bragg reflector (DBR)[16], photonic crystal (PhC) cavity[17,18], and fiber Bragg grating (FBG)[19–23] have been proposed and demonstrated. The PhC and FBG cavity formation on the ONF has been demonstrated via two techniques: one is the direct fabrication of nanocavities on the ONF using the focused ion beam (FIB) milling technique[24–27] and femtosecond laser ablation method[28,29], and the other is using external grating over the ONF[2,30], which does not directly fabricate on the ONF. But, in this case, the coupling efficiency is limited to 75-80 % only[21,22].

However, one of the most matured and commercially available fiber systems like Tilted Fiber Bragg Grating (TFBG) has not been explored on the ONF. The TFBG fabrication uses laser writing on a doped fiber by an interference pattern. This flexible approach allows changing of the periods as well as tilt angles conveniently. For a large number of identical grating, the interference pattern is generated by a diffractive phase mask located close to the fiber[31]. The tilt angle is monitored by rotating either the phase mask or the fiber[32]. The tuning of the resonance wavelength has not been experimentally

*Corresponding author: (E-mail: rjha@iitbbs.ac.in)

demonstrated, but two possible ways have been proposed. One is to accurately control the diameter of ONF so that the effective refractive index of the guided mode changes[33,34]. Another one is by changing the relative angle between the gratings and ONF[2,35,36]. By tilting the angle of gratings, the resonance angle can be tuned up to± 50 nm[35].

In this work, we have reported a new technique using tilted grating in an optical nanofiber called tilted nanofiber Bragg grating (TNFBG) as an efficient single-photon collector from a single QE. This structure is designed by three-dimensional finite-difference time-domain (3D-FDTD) simulations to enhance the spontaneous emission decay rate from a QE and maximize the coupling efficiency into the fiber-guided modes. Here, we systematically analyze the polarization-dependent cavity characteristics and spontaneous emission characteristics of TNFBG. We show that the coupling efficiency from a single QE can reach as high as ~ 90% with the Purcell factor can be as high as ~ 65.The maximum degree of polarization of the single photons has been calculated as high as 96%. The results show a 10-fold enhancement factor from a QE in the cavity center compared with the cavity surface. With these properties, TNFBG will improve single photon sources for nanophotonic quantum networks and will enable the efficient employment of important devices needed for quantum information processing.

In this study, we designed the TNFBG for an operating wavelength of around 795 nm, the typical emission wavelength of Rubidium D_1 line resonance. Fig. 1 shows the conceptual diagram of TNFBG. The enlarged portion shows the waist region where two sets of TFBG mirrors are considered by maintaining a

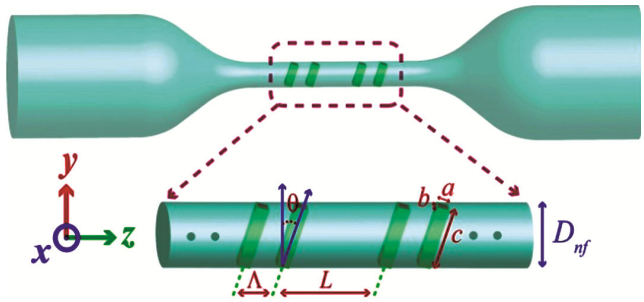

Fig. 1 — Conceptual diagram of TNFBG. Schematic diagram of an SMF tapered to nano range with tilted gratings on both sides of a cavity. The enlarged view shows the TNFBG in the ONF having defined parameters *L*, D_{nf}, θ, *a, b, c,*and Λ.All gratings are tilted by an angle,θ about the *y*-axis.For this case, $N = 25$ on either side of the *L*. Note that the number of grating periods shown in the schematic is less than that in the actual simulation.

defect length (*L*). In this proposed structure, an air-clad silica ONF having a diameter D_{nf}= 800 nm is considered with a refractive index of 1.450. Here, the cavity is formed by etching rectangular gratings having etched width $a = b =$ 120 nm, etched depth c = 810 nm with grating pitch Λ = 310 nm, defect length $L = 13\Lambda/2 = 2.015$ μm, etched grating period numbers N = 25on either side of the defect region, and tilt angle θ= 15° relative to the fiber cross-section along *y*-axis plane is considered. The grating pitch (Λ) of this TNFBG structure is determined from the Bragg resonance condition[32,37],

$$\lambda_r = \left[n_{eff}^{core}(\lambda_r) + n_{eff}^{s}(\lambda_r) \right] \Lambda / \cos(\theta), \qquad ...(1)$$

here, λ_r is Bragg resonance wavelength, $n_{eff}^{core}(\lambda_r)$ is the effective index of fundamental core mode, and $n_{eff}^{s}(\lambda_r)$ is the effective index of mode "*s*" at the same wavelength, λ_r.

2 Results and Discussion

To analyze the cavity characteristics of the proposed system, light from a broadband mode source is considered to be coupled into the TNFBG. Here, two orthogonal polarization modes of light are considered, *i.e.*, X-polarized (X-pol) and Y-polarized (Y-pol) modes, which are perpendicular and parallel to the grating plane, respectively as delineated in the conceptual diagram. Figs. 2(a) and 2(b) show the transmission and reflection spectra of TNFBG. The green dashed line shows the stop band spectra for L = 0 μm. Here, almost 0% (98%) of light is transmitted (reflected), respectively[23]. The central wavelength and width of the stop band are 794 nm and 37 nm, respectively. To make the TNFBG a resonant cavity, an optimized value of L = 2.015 µm is considered in the middle of two symmetric tilted gratings having period numbers N = 25 on either side of the cavity. There is a sharp resonance peak is observed in the middle of the stop band of the transmission and reflection spectra for both X-pol and Y-pol lights. The proposed TNFBG structure has resonance wavelengths (λ_r) that are close to the emission wavelength of the single QE (nearly795 nm). The λ_r of cavity resonance mode is 793.74 nm (798.60 nm) for X-pol (Y-pol) light, respectively. The resonance peaks (dips) of X-pol and Y-pol lights in transmission (reflection) spectra are separated by 5.14 nm, and the on-resonance transmittance (T_0) of 0.70 (0.89) and the

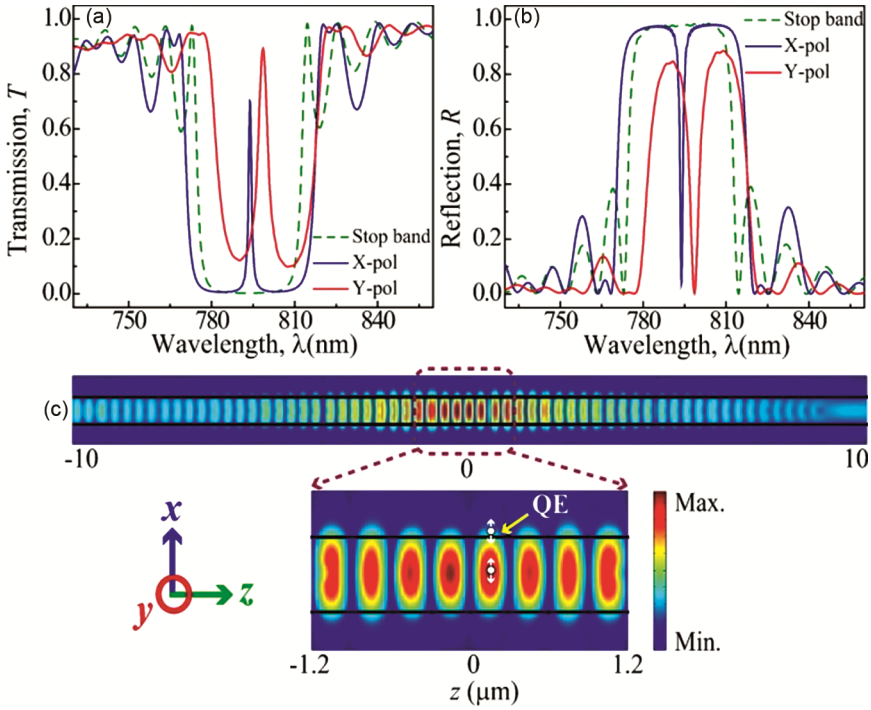

Fig. 2 — Cavity characteristics. (a) and (b) Show the simulated transmission (T) and reflection (R) spectra of TNFBG, respectively, for the stop band (green dashed lines), X-pol (blue line), and Y-pol (red line) lights.(c) Electric field distribution along the TNFBG for X-pol light. The enlarged region shows an expanded view near the cavity region. Black straight lines mark the position of the edges of the ONF. Two locations of QE (white circle with arrow) are considered: in the center and on the surface.

cavity linewidths of $\Delta\lambda_x(\Delta\lambda_y)$ = 1.1 nm (3.7 nm) are estimated for X-pol (Y-pol) light, respectively. The cavity the linewidth of the resonance peak for X-pol light is sharper than Y-pol light because X-pol light experiences larger index modulation by the TNFBG[21,22]. So, the quality factor (Q-factor = $\lambda_r/\Delta\lambda$) is estimated for X-pol (Y-pol) light is 722 (216), respectively. The X-pol light has a higher Q-factor as compared to the Y-pol light. Here, the cavity wavelength (λ_r) can be tailored and controlled by changing the grating pitchΛ and it shows a redshift as Λincreases. The dissipative nature of resonance mode makes it different from other modes.

Further, Fig. 2(c) shows the electric field intensity $|E|^2$ distribution along the TNFBG for X-pol light at the λ_r = 793.74 nm. The expanded region shows the field distribution close to the cavity region. One can clearly see the periodic field intensity pattern formed due to the standing wave, with high (low) intensity at the anti-node (node) position, respectively with a period of 300 nm. It can be seen that a part of the field intensity also lies outside the TNFBG. To measure the spatial confinement of the electromagnetic field in the cavity, one can calculate the effective cavity mode volume V_{eff}[38],

$$V_{eff} = \frac{\int_v \varepsilon(r)|E(r)|^2 d^3r}{\max[\varepsilon(r)|E(r)|^2]}, \quad ...(2)$$

where, $\varepsilon(r)$ is the dielectric constant of the fiber, and $E(r)$ is the electric field. From Eq. (2), the V_{eff} is calculated to be as small as 0.56 μm^3 (0.66 μm^3) for X-pol (Y-pol) light with N = 25 on each side of the cavity of TNFBG. However, it can be tailored with the value of N[23]. Lower the mode volume, higher the enhancement in the spontaneous emission decay rate. So, TNFBG has high Q-factors, low V_{eff}, and lossless coupling eventually to the SMF with a sharp resonance peak, these properties make TNFBG an efficient platform for single photon collection.

Now, to see the effect of the tilt angle (θ) of the grating on the cavity responses; θ is varied from 1° to 31° in steps of 5°. Fig. 3(a) shows the change in λ_r and Q-factor with θ for X-pol light. Inset shows the variation in transmission resonance spectra with θ.As can be seen with the increase in θ, λ_r shows a blue shift in wavelength with increased transmittance, which can also be verified from the inset figure. The λ_r-value can tune up to ~ 10 nm with a variation of θ up to 30°. The Q-factor also decreases with an increase in θ, this is due to an increase in cavity

linewidth. Maximum Q-factor ~ 1000 can be achieved at θ = 1°.

Here, λ_r is the wavelength at which the maximum reflection occurs, we can define T_0 and R_0 as the on-resonance transmittance and reflectance at λ_r, respectively. Also, the optical loss due to gratings at λ_r can be defined as, $L_0 = 1 - R_0 - T_0$[30]. Fig. 3(b) shows the simulated T_0 (blue squares), R_0 (green circles), and L_0 (red triangles)- values as a function of θ. One can see that the T_0 (R_0&L_0) - values increase (decrease) with increasing the θ, respectively. This signifies that, by tilting the grating angle, optical loss of the cavity decreases, and transmittance increases.This resulting the maximum coupling of single photons from a QE, which is essential for an efficient photonic device.

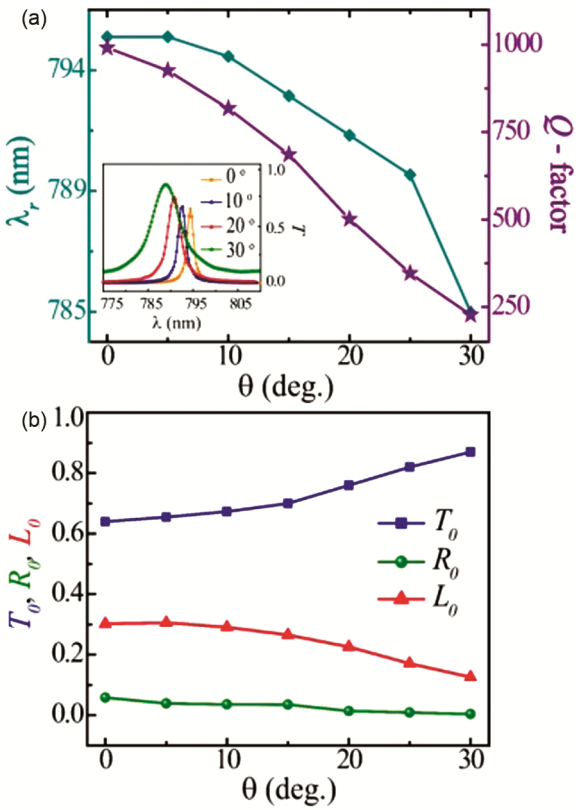

Fig. 3 — Effect of tilt angle, θ. (a) Change in resonance wavelength (λ_r) and Q-factor with θ, varies from 1° to 31° in steps of 5°for X-pol light. Inset shows the variation in transmission resonance spectra with θ. (b) Shows the simulated on-resonance transmittance, T_0 (blue squares), reflectance, R_0 (green circles), and optical loss L_0 (red triangles)- values as a function of θ. The solid lines connect the points to guide the eye.

Now to see the optical characteristics of the TNFBG + QE hybrid system, a QE is placed in two different positions *i.e.*, at the center and surface of the TNFBG cavity antinode position as shown in the enlarged region of Fig. 2(c). To place the QE in the center position, a small hole can be created at that particular position[23,39,40]. In FDTD simulations, a QE is considered as an electric dipole having three orthogonal polarizations *i.e.*, X-pol, Y-pol, and Z-pol[12], as depicted in Fig. 1. In Figs. 4(a) and 4(b),we show simulated PL intensity spectra (I) recorded through the guided modes of an ONF from a QE placed at the center and surface of the field antinode position having X- (blue solid line), Y- (red dashed line), and Z-(green dotted line)polarizations, respectively. Both the PL spectra have enhancement peaks at 794.7 nm (796.8 nm) for X-pol (Y-pol) QE placed at center and surface positions, respectively. Both enhancement peaks are separated by 2.1 nm. The lack of coupling for the Z-pol QE is due to the relative phase shift of the z- component of the TNFBG cavity modes[2,20]. The QE enhancement peaks have line widths of 0.9 nm (3.04 nm) at the center position and 1.07 nm (3.49 nm) at the surface position for X-pol (Y-pol) QE, respectively. The PL intensity spectrum of X-pol shows a higher and sharper peak than that of the Y-pol due to the higher Q-factor. The

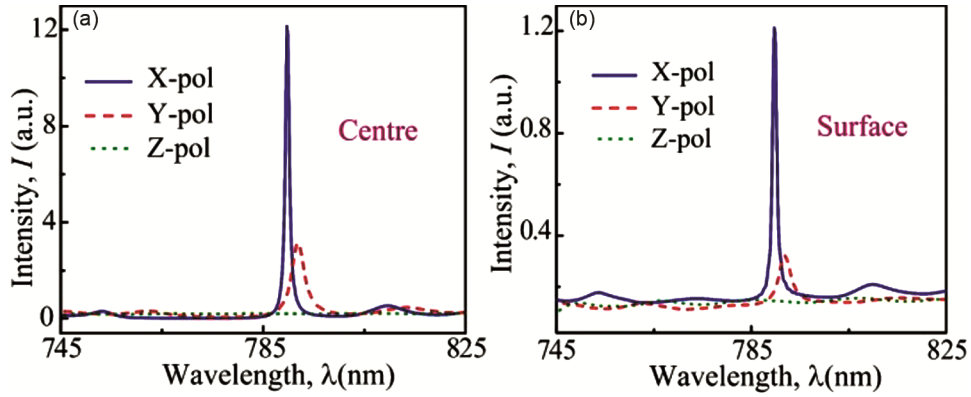

Fig. 4 — Photoluminescent (PL) spectra. (a) and (b) Show simulated PL intensity spectra from a QE placed at the center and surface of the cavity for X- (blue solid line), Y- (red dashed line), and Z-polarized (green dotted line) dipole sources, respectively.

intensity of PL spectra (enhancement factor) for QE at the center position has a 10-fold enhancement than the QE at the surface position because electric field intensity at the surface position is significantly low as compared to the center position as shown in Fig. 2(c).

Now to verify the spontaneous emission characteristics and coupling mechanism of the QE in the presence of TNFBG, the QE is placed at different positions in the cavity. The maximum field inside the cavity will enhance the spontaneous emission rate of the QEs. Further, QE placed at the field antinode position in an optical cavity will experience a medium-enhanced spontaneous emission rate relative to that in a homogeneous medium based on the Purcell effect[41]. The magnitude of enhancement of QE is given by Purcell factor (F) as[42],

$$F = \frac{3}{4\pi^2}\left(\frac{\lambda_r}{n_{eff}}\right)^3\left(\frac{Q}{V_{eff}}\right), \quad ...(3)$$

where n_{eff} is the effective mode index inside the cavity. Also, Fermi's golden rule dictates that the transition rate for the atom-vacuum (or atom-cavity) system is proportional to the initial and final photon states of the system with a weak perturbation as well as the local density of state (LDOS) as[43],

$$\Gamma_{i\to f} = \frac{2\pi}{\hbar}\left|\langle f|H'|i\rangle\right|^2 \rho\left(E_f\right), \quad ...(4)$$

where i and f are the initial and final states, H' is perturbed Hamiltonian, ρ is the density of states, and E_f is the final energy state. In a cavity system, at resonance, the density of the final state is enhanced. Therefore, the spontaneous emission decay rate (γ)of a two-level QE in the presence of the TNFBG is given by[43],

$$\gamma = \frac{\pi\omega_0}{3\hbar\varepsilon_0}|p|^2\ \rho_p(r_{0,}\omega_0),$$

$$\rho_p(r_{0,}\omega_0) = \frac{6\omega_0}{\pi c^2}\left[n_p.\mathrm{Im}\left\{\vec{G}\left(r,r_0;\omega_0\right)\right\}.n_p\right], \quad ...(5)$$

where ω_0 is the transition angular frequency, $|p|^2$ is the transition dipole moment, $p = |p|n_p$ is the dipole moment of an emitter and n_p is the unit vector in the direction of p. $\vec{G}\left(r,r_0;\omega_0\right)$ is the Dydics Green's function is defined by the electric field at a point r generated by a point source at point $r_0$with dipole moment $p$as,

$$G\left(r,r_0\right) = \frac{\varepsilon_0\varepsilon_r c^2}{p\,\omega_0^2}E\left(r\right), \quad ...(6)$$

where $\varepsilon_0$and ε_r are the permittivity of air and relative permittivity of the medium.

Here, the Purcell factor ($F = P/P_0$) and coupling efficiency ($\beta = P_c/P$) is calculated using FDTD simulations using a dipole source and power monitors. Where, P, P_0, and P_c are the total power emitted by the dipole source, in the presence of the TNFBG, to the vacuum environment, and coupled into the guided modes, respectively[23]. Further, the degree of polarization (DOP)of single photons in the TNFBG system is determined by DOP = $(I_x + I_y - I_z)/(I_x + I_y + I_z)$, where I_j ($j = x, y, z$) is the proportion of the emitted light intensity coupled to the ONF for a dipole source polarized along the j-axis[44,45].

To study the Purcell enhancement and coupling mechanism QE with TNFBG, Fig. 5 characterizes the F, and β for a QE positioned at the different locations on the cavity along the z-axis. Figs. 5 (a, b) and 5 (c, d) show variations of optical responses *i.e.*, (F,β) on the position Δz of the QE at the center and surface of the TNFBG cavity, respectively for X- (blue squares), Y- (red circles), and Z- (green triangles) polarized dipole sources. One can place a QE at the center position by directly embedding in the core[12,21,46], or by making a hole in the ONF[22,23,39]. For atoms, a magneto-optical trap (MOT)[47,48], and an optical tweezer-based trapping scheme[49] have been used. To place a QE on the surface position of the ONF, well-established techniques are developed such as a sub-pico-liter needle-dispenser[8], and more deterministically by atomic force microscope (AFM) techniques[50,51].

As can be clearly seen from Fig. 5, all the spontaneous emission responses of QE, *i.e.*, F and β show an oscillating behaviour with a period of 300 nm on both sides of the zero position ($\Delta z = 0$) of the TNFBG cavity for the center and surface positions, for all polarizations. In case of X-pol and Y-pol, QEs have been assumed to be placed 170 nm away from $\Delta z = 0$. It is observed that F and β increase as the electric field intensity is maximum at that point (anti-node position), as shown above in Fig. 2(c). However, in the case of Z-pol, maximum F and β can be observed at the node position butX- and Y-pol modes

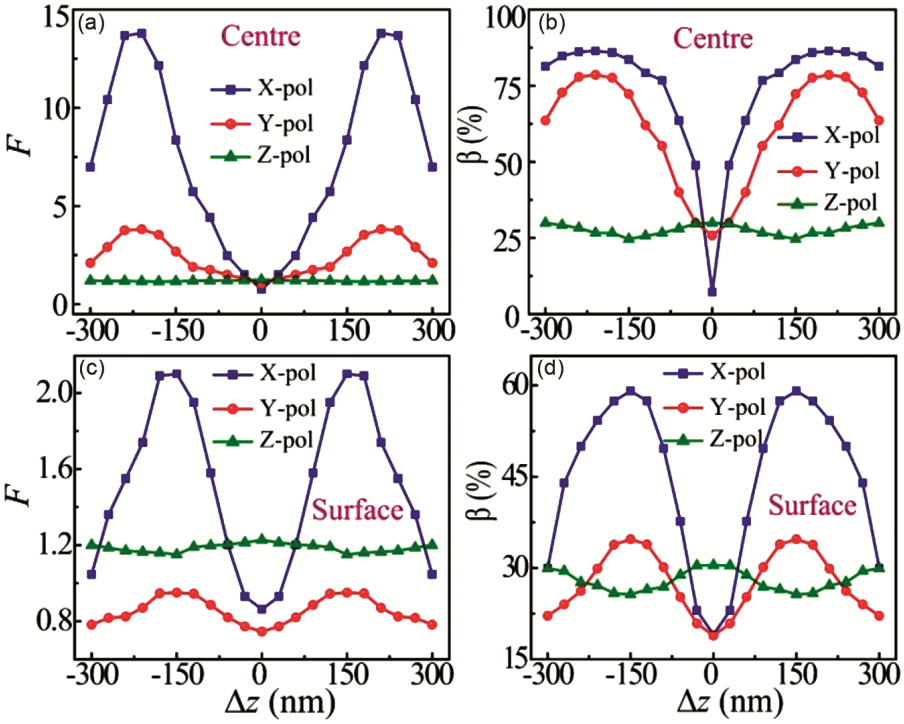

Fig. 5 — Effect of QE position. (a, b) and (c, d) show variations of optical responses *i.e.*, (F,β) on the position Δz of the QE at the center and surface of the TNFBG cavity, respectively for X- (blue squares), Y- (red circles), and Z- (green triangles) polarized dipole sources. The solid lines connect the points to guide the eye.

are completely suppressed at this position. This is due to the relative phase shift of the Z-component of the TNFBG cavity mode as shown in Fig. 5[2,52,53].

From Fig. 5 the peak F and β at the anti-node (node) position of the center location of the cavity are found to be 13.8 (0.75), 3.8 (1), 1.16 (1.24) and ~ 90% (7.2%), 78% (25%), 24% (30%) for the X-, Y-, and Z-pol, respectively. Similarly, the peak F, and β at the anti-node (node) position of the surface location of the cavity are found to be 2.1 (0.86), 0.95 (0.74), 1.15 (1.23) and ~ 60% (19%), 35% (18%), 25.6% (30%) for the X-, Y-, and Z-pol, respectively. The F and β of both polarized QEs are larger at the center than that for the emitter on the surface of the TNFBG, which mimics the electric field intensity as shown in Fig. 2(c). From this analysis, it is inferred that X-pol QE has higher F and β both at the surface and center positions because X-pol light has a higher Q-factor than the other polarizations. Compared with QE on the center of TNFBG, the F and β, increase by at least 6.6-fold (4-fold) and 1.5-fold (4.1-fold) for X-pol(Y-pol) QE, respectively than the surface. From these results, DOP can be calculated as ~ 96% (68%) for QE at the center (surface) position, respectively.

Further to see the grating strength, the number of grating periods (N) of TNFBG varies. Fig. 6 (a) and 6(b) represent the dependence of F (blue circles) and β (red stars) on the N = 5 to 85 at the interval of 5 for X-pol and Y-pol QEs at the center position, respectively. One can see that with the increase in N-values, F increases and saturates for N = 60 for X-pol QE, whereas for Y-pol, it saturates to lower F value at N = 80. At these values of N, Q-factor saturates to the scattering limited Q-value, and hence F also saturates[23,54] as per Eq.3. But, one can readily see that the β-value shows a rising and then declining trend with increasing N-value for both the polarized QEs. Maximum β~ 90 % (86%) at N = 25 (40) is obtained for X-pol (Y-pol) QE, respectively. For much higher values of N, β reduces to 0% due to the increased grating loss for both the polarized QEs.

It is important to mention that, ONFs are very delicate, mechanically unstable and therefore making gratings on them is a challenging task unlike larger conventional fiber. Experimentally FBGs were fabricated on ONF using a focused ion beam milling technique[19,26]. Further, large-scale grating production will also weaken ONF and could result in greater losses. In our proposed design, with the thicker fiber (0.8 μm) and lower number of gratings, coupling efficiency is as high as 90% makes the proposed system more desirable.

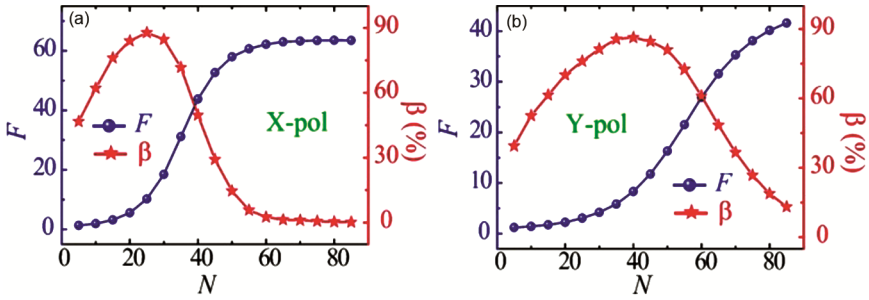

Fig. 6 — Effect of grating strength (N). (a) and (b) Show the dependence of F (blue circles) and β (red stars) on the period numbers $N = 5$ to 85 at an interval of 5 for X-pol and Y-pol QEs at the center position, respectively. The solid lines connect the points to guide the eye. Note that this N refers to one side of the TNFBG.

3 Conclusion

In summary, we have reported a new avenue for quantum photonics, and cavity QED applications. We show that the coupling efficiency from single emitters can reach as high as ~ 90% with the Purcell factor can be as high as ~ 65.The maximum degree of polarization of the single photons has been calculated as high as 96%.The results show a 10-fold enhancement factor for QE in the cavity center compared with the cavity surface. We have shown the electric field enhancement in the cavity region and coupling of the florescent photons from the QE at different positions into the guided mode of TNFBG. This structure would help to realize quantum information devices, such as quantum memories, fiber-integrated single-photon sources, & light-matter interaction for future quantum technologies.

Acknowledgments

RJ acknowledges the support of the SERB STAR Fellowship (STR/2020/000069) from Govt. of India.

References

1 Kimble H J, *Nature*, 453 (2008) 1023.
2 Yalla R, Sadgrove M, Nayak K P & Hakuta K, *Phys Rev Lett*, 113 (2014) 143601.
3 Rajasree K S, T Ray, Karlsson K, Everett J L & Chormaic S N, *Phys Rev Res*, 2 (2020) 12038.
4 Nayak K P, M Sadgrove, Yalla R, Kien F L & Hakuta K, *J Opt*, 20 (2018) 73001.
5 Lou N, Jha R, Domínguez-Juárez J L, Finazzi V, J Villatoro, Badenes G & Pruneri V, *Opt Lett*, 35 (2010) 571.
6 Kumar A, Sahu S & Jha R, *J Phys D Appl Phys*, 55 (2022) 405102.
7 Morrissey M J, Deasy K, Frawley M, Kumar R, Prel E, Russell L, Truong V G & Chormaic S N, *Sensors*, 13 (2013) 10449.
8 Yalla R, Kien F L, Morinaga M & Hakuta K, *Phys Rev Lett*, 109 (2012) 063602.
9 Shafi K M, Nayak K P, Miyanaga A & Hakuta K, *Appl Phys B Lasers Opt*, 126 (2020) 58.
10 Stiebeiner A, Rehband O, Garcia-Fernandez R & Rauschenbeutel A, *Opt Express*, 17 (2009) 21704.
11 S Murmu, Kumar A & Jha R, *Adv Quantum Technol*, 5 (2022) 2100160.
12 Almokhtar M, Fujiwara M, Takashima H & Takeuchi S, *Opt Express*, 22 (2014) 20045.
13 Murmu S, Kumar A & Jha R, *J Opt Soc Am B*, 38 (2021) F170.
14 Schell A W, Takashima H, Tran T T, Aharonovich I & Takeuchi S, *ACS Photon*, 4 (2017) 761.
15 Kien F Le, Gupta S D, Balykin V I & Hakuta K, *Phys Rev A - At Mol Opt Phys*, 72 (2005) 032509.
16 Li S, Chen Y, Shang X, Yu Y, Yang J, Huang J, Su X, Shen J, Sun B, Ni H, Su X, Wang K & Niu Z, *Nanoscale Res Lett*, 15 (2020) 145.
17 Nayak K P, Zhang P & Hakuta K, *Opt Lett*, 39 (2014) 232.
18 Keloth J, Nayak K P & Hakuta K, *Opt Lett*, 42 (2017) 1003.
19 Kien F L, Nayak K P & Hakuta K, *J Mod Opt*, 59 (2012) 274.
20 Kien F L & Hakuta K, *Phys Rev A*, 80 (2009) 53826.
21 Takashima H, Fujiwara M, Schell A W & Takeuchi S, *Opt Express*, 24 (2016) 15050.
22 Li W, Du J & Chormaic S N, *Opt Lett*, 43 (2018) 1674.
23 Sahu S, Nayak K P & Jha R, *J Opt*, 24 (2022) 115401.
24 Romagnoli P, Maeda M, J Ward M, Truong V G & Chormaic S N, *Appl Phys B Lasers Opt*, 126 (2020) 111.
25 Nayak K P, Kien F L, Kawai Y, Hakuta K, Nakajima K, Miyazaki H T & Sugimoto Y, *Opt Express*, 19 (2011) 14040.
26 Li W, Du J, V Truong G & Chormaic S N, *Appl Phys Lett*, 110 (2017) 253102.
27 Schell A W, Takashima H, Kamioka S, Oe Y, Fujiwara M, Benson O & Takeuchi S, *Sci Rep*, 5 (2015) 9619.
28 Nayak K P, Wang J & Keloth J, *Phys Rev Lett*, 123 (2019) 213602.
29 Nayak K P, Keloth J & Hakuta K, *J Vis Exp*, 2017 (2017) e55136.
30 Sadgrove M, Yalla R, Nayak K P & Hakuta K, *Opt Lett*, 38 (2013) 2542.
31 Hill K O, Malo B, Bilodeau F, Johnson D C & Albert J, *Appl Phys Lett*, 62 (1993) 1035.
32 Albert J, Shao L Y & Caucheteur C, *Laser Photon Rev*, 7 (2013) 83.
33 Keloth J, Sadgrove M, Yalla R & Hakuta K, *Opt Lett*, 40 (2015) 4122.
34 Zhu M, Wang Y-T, Sun Y-Z, Zhang L & Ding W, *Opt Lett*, 43 (2018) 559.

35 Yalla R & Hakuta K, *Appl Phys B Lasers Opt*, 126 (2020) 187.
36 Dai H, Zhong Y, Wu X, Hu R, Wang L, Zhang Y, Fan G, Hu X, Li J & Yang Z, *J Electroanal Chem*, 810 (2018) 95.
37 Chen C, Caucheteur C, Mégret P & Albert J, *Meas Sci Technol*, 18 (2007) 3117.
38 Srinivasan K, Borselli M, Painter O, Stintz A & Krishna S, *Opt Express*, 14 (2006) 1094.
39 Wang X, Zhang P, Li G & Zhang T, *Opt Express*, 29 (2021) 11158.
40 Daly M, Truong V G, Phelan C F, Deasy K & Chormaic S N, *New J Phys*, 16 (2014) 53052.
41 Purcell E M, *Phys Rev*, 69 (1946) 681.
42 Rao V S C M & Hughes S, *Phys Rev B - Condens Matter Mater Phys*, 75 (2007) 205437.
43 Novotny L & Hecht B, (Cambridge university press, 2012).
44 Shafi K M, Yalla R & Nayak K P, *Phys Rev Appl*, 19 (2023) 34008.
45 Sugawara M, Y Xuan, Mitsumori Y, Edamatsu K & Sadgrove M, *Phys Rev Res*, 4 (2022) 43146.
46 Gaio M, Moffa M, Castro-Lopez M, Pisignano D, Camposeo A & Sapienza R, *ACS Nano*, 10 (2016) 6125.
47 Nieddu T, Gokhroo V & Chormaic S N, *J Opt*, 18 (2016) 53001.
48 Das M, Shirasaki A, Nayak K P, Morinaga M, Kien F L & Hakuta K, *Opt Express*, 18 (2010) 17154.
49 Nayak K P, Wang J & Keloth J, *Phys Rev Lett*, 123 (2019) 213602.
50 Liebermeister L, Petersen F, Münchow A V, Burchardt D, Hermelbracht J, Tashima T, Schell A W, Benson O, Meinhardt T, Krueger A, Stiebeiner A, Rauschenbeutel A, Weinfurter H & Weber M, *Appl Phys Lett*, 104 (2014) 031101.
51 Yalla R, Kojima Y, Fukumoto Y, Suzuki H, Ariyada O, Shafi K M, Nayak K P & Hakuta K, *Appl Phys Lett*, 120 (2022) 241102.
52 Kien F L & Hakuta K, *Phys Rev A - At Mol Opt Phys*, 79 (2009) 053826.
53 Yalla R R, Shafi K M & Hakuta K, *Phys Soc Jpn*, 73 (2018) 206.
54 Yalla R, Shafi K M, Nayak K P & Hakuta K, *Appl Phys Lett*, 120 (2022) 071108.